

# Transient-state kinetic analysis of multi-nucleotide addition catalyzed by RNA polymerase I

Zachariah M. Ingram, David A. Schneider, 2,\* and Aaron L. Lucius 1,\*

<sup>1</sup>Department of Chemistry and <sup>2</sup>Department of Biochemistry and Molecular Genetics, University of Alabama at Birmingham, Birmingham, Alabama

ABSTRACT RNA polymerases execute the first step in gene expression: transcription of DNA into RNA. Eukaryotes, unlike prokaryotes, express at least three specialized nuclear multisubunit RNA polymerases (Pol I, Pol II, and Pol III). RNA polymerase I (Pol I) synthesizes the most abundant RNA, ribosomal RNA. Nearly 60% of total transcription is devoted to ribosomal RNA synthesis, making it one of the cell's most energy consuming tasks. While a kinetic mechanism for nucleotide addition catalyzed by Pol I has been reported, it remains unclear to what degree different nucleotide sequences impact the incorporation rate constants. Furthermore, it is currently unknown if the previous investigation of a single-nucleotide incorporation was sensitive to the translocation step. Here, we show that Pol I exhibits considerable variability in both  $k_{max}$  and  $K_{1/2}$ values using an in vitro multi-NTP incorporation assay measuring AMP and GMP incorporations. We found the first two observed nucleotide incorporations exhibited faster  $k_{max}$ -values ( $\sim 200~s^{-1}$ ) compared with the remaining seven positions ( $\sim 60~s^{-1}$ ). Additionally, the average  $K_{1/2}$  for ATP incorporation was found to be approximately threefold higher compared with GTP, suggesting Pol I has a tighter affinity for GTP compared with ATP. Our results demonstrate that Pol I exhibits significant variability in the observed rate constant describing each nucleotide incorporation. Understanding of the differences between the Pol enzymes will provide insight on the evolutionary pressures that led to their specialized roles. Therefore, the findings resulting from this work are critically important for comparisons with other polymerases across all domains of life.

SIGNIFICANCE RNA polymerase I (Pol I) is one of three known nuclear RNA polymerases and is responsible for the synthesis of the ribosomal RNA, an essential step in ribosome biogenesis. Previously, we published a minimal kinetic mechanism describing single-nucleotide addition catalyzed by Pol I, in which a single rate-limiting step of  $\sim$ 180 s<sup>-1</sup> was observed. Here, we extend those findings and present an examination of nine sequential nucleotide additions using transient state kinetics. This work has implications in connecting single-nucleotide incorporation rate constants with observed rate constants garnered from averaging over hundreds of nucleotide incorporations. Surprisingly, we found high variability between each incorporation. Finally, the findings presented here are impactful in identifying unique differences between the nuclear RNA polymerases.

#### INTRODUCTION

The three nuclear multisubunit DNA-dependent RNA polymerases (RNAP) (Pols I, II, and III) are known to have specialized roles in gene expression. Pol I synthesizes the majority of the ribosomal RNA, Pol II synthesizes messenger RNA and most regulatory noncoding RNAs, and Pol III primarily synthesizes the transfer RNA and the 5S ribosomal RNA. Strikingly, although having unique roles, the three polymerases exhibit considerable sequence

Submitted March 5, 2021, and accepted for publication September 7, 2021.

\*Correspondence: dschneid@uab.edu or allucius@uab.edu

Editor: Smita S. Patel.

https://doi.org/10.1016/j.bpj.2021.09.008

© 2021 Biophysical Society.

conservation (1). Five of the 14, 12, and 17 subunits present in Pols I, II, and III, respectively, are identical. Sequence alignments focused on the trigger loop portions of the three polymerases shows extensive conservation (2,3). Reasonably, these observations all suggest a similar mechanism of transcription would describe all three polymerases. However, the small molecule  $\alpha$ -amanitin has been shown to specifically inhibit transcription catalyzed by Pol II. Likewise, tagetitoxin has been shown to specifically inhibit Pol III without significantly impacting RNA synthesis catalyzed by Pol I and Pol II (4). The specificity of these inhibitors suggests that although structurally similar, the three polymerases evolved mechanisms that are functionally distinct.



The hypothesis that the three polymerases have functionally distinct mechanisms is further supported by an investigation in which a known gain of function mutation for Pol II (Pol II: *rpb1-E1103G*) was engineered into Pol I (Pol I: *rpa190-E1224G*) and resulted in an opposite phenotype (2). The point mutations discussed are in the trigger loop, a region that is conserved among multisubunit RNAPs (5–8). A further characterization of nucleotide addition catalyzed by this Pol I variant suggests that the decrease in function is a result of a reduction in the covalent bond formation step (9). These findings demonstrate clear differences in the kinetic mechanisms of Pols I and II and indicate that independent kinetic characterizations of each enzyme are necessary to gain insight into how each polymerase evolved to fulfill its respective role (10).

Experiments have been performed, both in vitro and in vivo, to probe the kinetic mechanism of nucleotide addition catalyzed by Pol I. Two in vitro experiments found the average maximal rate of nucleotide addition by Pol I to be  $\sim$ 60 nt s<sup>-1</sup> after averaging over hundreds of nucleotide incorporations (9,11). Consistently, an in vivo measurement reported a rate of  $50 \pm 20$  nt s<sup>-1</sup> (12). We performed transient state kinetics to elucidate a minimal kinetic model that described single adenosine monophosphate (AMP) addition by Pol I (13). The model suggests that the rate-limiting step is the formation of the covalent bond between the nascent RNA and the incoming AMP and has a value of  $\sim$ 180 s<sup>-1</sup>. This rate constant is threefold higher than the average maximal rate of nucleotide addition observed in the multinucleotide addition experiment both in vivo and in vitro.

If Pol I single-nucleotide incorporation is rate limited by a single kinetic step with a rate constant of 180 s<sup>-1</sup> and averaging over thousands of incorporations reveals that incorporation occurs at  $\sim 60$  nt s<sup>-1</sup>, then why is there such a large disparity between the two measurements (9,13)? How are the kinetics of a single-nucleotide incorporation related to the repeating cycles of multiple nucleotide incorporations? To address these questions, here, we sought to examine the kinetics of nucleotide addition catalyzed by Pol I in the context of multiple incorporations. Furthermore, these experiments will reveal if differences in the incorporation sequence impact the kinetics of each addition. To this end, we used transientstate kinetic techniques to interrogate the mechanism of incorporation of nine sequential nucleotide additions. The strength of this strategy is that, in a single experiment, we acquire nine time courses corresponding to the rise and fall of eight intermediate incorporations and the formation of final product. Consequently, each time course provides a constraint on the elementary rate constant for the formation and disappearance of the n-th intermediate and the formation of the (n + 1) product. Detailed analysis of these time courses shows substantial variability in the maximal rate constant and binding affinity at each of the nine incorporation positions. Although the rate constants and NTP binding affinities are variable at each position, they fall within a range that would yield the expected average that was previously seen with longer templates,  $(67 \pm 4) \, \mathrm{s}^{-1}$  and  $(142 \pm 22) \, \mu \mathrm{M}$  (9). However, the first incorporation was observed to be much faster than the average over many incorporations, which agrees with our previously reported single-nucleotide incorporation experiments. Surprisingly, the second incorporation in these experiments was also observed to be much faster than all subsequent additions.

#### **MATERIALS AND METHODS**

## **Buffers**

All buffers and salt solutions were filtered using Millipore express plus vacuum-driven  $0.22~\mu m$  filters (MilliporeSigma, Billerica, MD) unless specified otherwise.

Nucleotide incorporation reactions were run in reaction buffer: (40 mM KCl, 20 mM Tris-Acetate (OAc) (pH 8.23) at 25°C, 2 mM dithiothreitol, 0.2 mg mL<sup>-1</sup> bovine serum albumin (BSA)).

#### **Proteins**

Pol I was purified from *Saccharomyces cerevisiae*, as described previously (14). For ease of purification, the cells expressed an FLAG-His6 tag on the C-terminus of A190 as the sole source of that subunit. Pol I is stored in 0.55 M K-OAc, 10 mM K-HEPES, 0.5 mM MgCl<sub>2</sub>, 45% (v/v) glycerol (pH 7.8); at  $-80^{\circ}$ C.

# Nucleotides, nucleic acids, heparin, and BSA

Preparation of nucleotides, nucleic acids, heparin, and BSA was described in detail previously (13). Nucleic acids were purchased from Integrated DNA Technologies (Cedar Rapids, IA). The template DNA sequence, nontemplate DNA sequence, and RNA primer are shown below. The location of the complementary sequences between the template DNA and the RNA primer are shown in bold.

Template DNA strand is coded as follows: 5'-ACCAGCAGGCCGATTG GGATGGGTATTCCCTCCTGCCTCTCGATGGCTGTAAGTATCCTAT

Nontemplate DNA strand is coded as follows: 5'-CCTATAGGATACTT ACAGCCATCGAGAGGCAGGAGGGAATACCCATCCCAATCGGCCT GCTGGT

RNA primer is coded as follows: 5'AUCGAGAGG

# Quench-flow time courses

Quenched flow time courses of multinucleotide incorporation reactions and electrophoresis, and quantification of gels were performed as previous described but with minor modifications (13). Previously, we only included ATP in the NTP syringe, whereas here, we are including both ATP and GTP. Previously, sodium acetate was added to the bottom buffer tank in the gel electrophoresis setup, and in this work, that was excluded. In the previously published manuscript, Bio-Rad Laboratories' software program Quantity One (Hercules, CA) was used to quantify the band densities in the polyacrylamide gel electrophoresis (PAGE) gels. In this investigation, the GE Healthcare software program ImageQuant TL (Cytiva, Marlborough, MA) was used.

In this experiment, two solutions were rapidly mixed together. The first solution contained the radiolabeled elongation complex. The concentration of the different components in this solution are shown below. The second syringe contained ATP, GTP, heparin, and  ${\rm Mg}^{2+}$ .

The concentration of both syringes shown below are premixing concentrations.

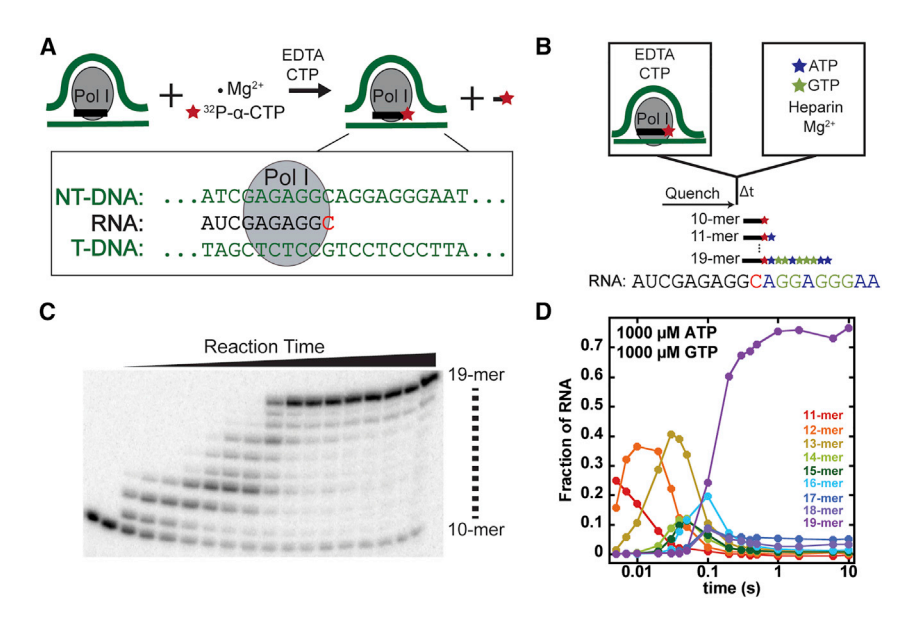


FIGURE 1 Illustrations of experimental design and example experimental data set. (A) Elongation complexes were mixed with  $\alpha$ -<sup>32</sup>P $\alpha$ -CTP and magnesium cofactor to label RNA primer. The sequence of the template DNA, RNA primer, and nontemplate DNA are displayed. A small fraction of GC dimer is also produced. (B) A schematic of a chemicalquenched flow is displayed. One of the two rapidly mixed components is the radiolabeled elongation complex that was produced in the previous step. The second mixture is composed of ATP, GTP, heparin, and Mg<sup>2+</sup>. The ATP, GTP, and Mg<sup>2+</sup> will be used to elongate the transcript from a 10-mer to a 19-mer, whereas the heparin will act as a trap. (C) Elongated RNA intermediates are separated using denaturing PAGE. This example image was generated from an experiment in which 1 mM ATP and 1 mM GTP were present. (D) The density of each band is quantified and used to calculate time courses for each RNA intermediate and the final RNA product. The lines connecting the time points here are present simply for visualization purposes. To see this figure in color, go online.

# Radiolabeled elongation complex syringe

The radiolabeled elongation complex syringe contained ≈16 nM Pol I, 162.75 nM RNA, 54.26 nM DNA-t, 162.75 nM DNA-nt, ≈5 nM  $\alpha$ -<sup>32</sup>P-CTP, 100  $\mu$ M Mg(OAc)<sub>2</sub>, 1.1 mM ethylenediamine teraacetic acid (EDTA) –  $K_3$ , 5  $\mu M$  unlabeled CTP.

#### NTP syringe

Adenosine triphosphate (ATP) and guanosine triphosphate (GTP) were at the concentrations indicated in the text, 18 mM mg(OAc)<sub>2</sub>, 0.05 mg/mL<sup>-1</sup> heparin.

Mixing in the chemical-quenched flow instrument is 1:1; thus, the final concentrations upon mixing are twofold lower than described above. Importantly, the final  $Mg(OAc)_2$  is 9 mM and the final EDTA –  $K_3$  is 0.55 mM.

# Data analysis

Parameter optimization was carried out using the MATLAB (MathWorks, Natick, MA) toolbox MENOTR (Multi-Start Evolutionary Nonlinear OpTimizeR). MENOTR is a set of scripts that have been developed to run on the MATLAB platform. The scripts optimize parameters using a hybrid genetic/non-linear least squares (NLLS) strategy (Ingram et al., manuscript in press). This parameter optimization method leverages the strengths of both analysis strategies while minimizing the respective inherent weaknesses. In this parameter optimization strategy "good" parameter values are first ascertained using a genetic algorithm. The "good" parameter values are then used as initial guesses in optimization routines using an NLLS algorithm. Optimizing parameters in this manner avoids NLLS from being trapped in a local minimum and increases the probability of reporting the "best" set of parameters possible.

Data sets composed of nine time courses (11-mer to 19-mer) were fit globally to the schemes presented in Fig. 2. The resultant best fit parameters were tabulated and reported for different concentrations of ATP and GTP. The  $k_{obs}$  values were determined from two to six independent experiments and subsequent fits. Fits of the  $k_{obs}$  secondary plots were performed using KaleidaGraph (Synergy Software, Reading, PA).

# **RESULTS**

Pol I catalyzed transcription was examined using a previously published promoter-independent in vitro transcription assay (13). This assay allows a user to monitor the elongation phase of RNA synthesis but does not report on the initiation or termination phases. As illustrated in Fig. 1 A, an elongation complex was first assembled using a 9-mer RNA primer, template DNA strand, nontemplate DNA strand, and Pol I enzyme. The elongation complex was then incubated with  $\alpha^{-32}$ P-CTP and Mg<sup>2+</sup> cofactor. In Fig. 1 A, a red star is used to denote the radiolabeled CTP, and the oligonucleotide sequences are shown. The elongation complex incorporated the radiolabeled CTP into the RNA but cannot add the next nucleotide, ATP, because it is absent from the reaction. In the absence of the next cognate nucleotide, Pol I will cleave two nucleotides from the 3' end of the primer producing a radiolabeled dimer RNA product (5'-GC). To halt both the nuclease activity and any additional nucleotide addition activity, EDTA was added to chelate the Mg<sup>2+</sup> cofactor. Excess unlabeled CTP was then added to the solution to guarantee that the observed signal will only come from elongation complexes, which incorporated the radiolabeled CTP before the addition of ATP and GTP.

An illustration of a chemical-quenched flow is shown in Fig. 1 B. The two boxes represent the two sample syringes. One syringe contained the radiolabeled elongation complex presented in Fig. 1 A. The second syringe contained ATP, GTP, excess Mg<sup>2+</sup>, and heparin. The contents of the two syringes were rapidly mixed, allowed to react for variable amounts of time before being quenched with 1 M HCl and expelled from the apparatus into a sample tube. During the incubation time, Pol I elongated the nascent transcript from a 10-nucleotide RNA (10-mer) to a 19-nucleotide RNA (19-mer) using the ATP, GTP, and Mg<sup>2+</sup>. Pol I stopped catalyzing nucleotide incorporation at the 19-mer position because UTP is absent from the reaction. Heparin is included in large excess so that any free Pol I will rapidly bind to heparin; thereby maintaining single turnover conditions with respect to the labeled elongation complex. As described above, in the absence of the next cognate nucleotide, Pol I is anticipated to cleave off a dinucleotide from the 3' end of the nascent RNA (9,10,13,15–17). Unlike the labeling conditions in which only CTP is present, under reaction conditions, the excised nucleotides can be reincorporated because three of the four nucleotides are present. The red star in Fig. 1 B corresponds to the radiolabeled CTP, and the blue and green stars correspond to the newly added AMP and GMP nucleotides, respectively. The final complete 19-mer RNA product sequence is shown at the bottom of Fig. 1 B.

The samples, corresponding to different reaction times, were then loaded into different lanes of a sequencing gel to separate the elongated RNA intermediates. A representative gel image from an experiment with saturating ATP and GTP (1 mM) is shown in Fig. 1 C. The first two lanes represent time zero and the next 16 lanes correspond to increasing reaction time. The pixel density for each band in Fig. 1 C was quantified and the fraction of RNA was calculated for each RNA intermediate. Fig. 1 D displays the resultant time courses for each intermediate and final product, 19-mer.

The next task was to identify a minimal kinetic model describing the experimental time courses. For each repeating cycle of nucleotide incorporation, the polymerase must bind a nucleotide, catalyze phosphodiester bond formation, release pyrophosphate, and translocate to the next position to catalyze the next incorporation. The kinetic time courses shown in Fig. 1 D will be sensitive to the slowest step or steps within each of those repeating cycles of nucleotide incorporation. Thus, we sought to determine the simplest kinetic mechanism that could simultaneously describe the rise and fall of each intermediate (11-mer to 18-mer) and final product (19-mer) formation. It is important to note that each intermediate time course (11-18)provides two constraints. The rising phase constrains the rate-limiting step for formation of that intermediate, and the decay phase constrains the rate-limiting step for the disappearance of that intermediate. The rate-limiting step for disappearance of a given intermediate, in principle, is the rate-limiting step for formation of the next intermediate. Consequently, the collection of all nine time courses provide substantial constraints for the model.

The simplest model, given by Scheme 1, assumes that a single rate-limiting step per incorporation cycle governs the formation of a given species and that step is the same for each species. Shown in Fig. 2, Scheme 1 contains a single repeating observed rate constant,  $k_{obs}$ , for nine sequential nucleotide additions. A set of simulated time courses, shown in Fig. 2 A, were generated to provide insight into the features present in time courses from Scheme 1 and aid in the analysis of the experimental time courses. The most notable features in the simulated time courses are that the time course of each inter-

mediate systematically shifts to the right with each incorporation, the peak maximal height decreases with each subsequent intermediate, and the maximal peak of the 19-mer time course approaches one. In contrast, the experimental data set shown in Fig. 1 D exhibits the right shift of the peak for each intermediate, but the maximal peak height does not systematically diminish with each intermediate as it does in the simulation. Moreover, the 19-mer approaches a maximum of  $\sim 0.8$ .

An additional global scalar was required to account for the final product, 19-mer, not plateauing at one as shown in Fig. 2 B. According to Scheme 1, all 10-mer that enters the reaction will become 19-mer, thus resulting in the 19-mer time course approaching 1 in Fig. 2 A. In reality, some fraction of the polymerase that was competently bound and able to radio label the RNA in the RNA/DNA hybrid likely dissociated before initiation of the reaction. This hypothesis is supported by the clear 10-mer band present in Fig. 1 C. to account for this change in the 19-mer plateau point, a scalar constant was incorporated to scale the amplitude.

To test Scheme 1, a global optimization across all nine time courses was performed. The parameters and global amplitude scalar were optimized and the best fit lines with experimental data are shown in Fig. 2 B. A resultant  $\chi^2$ -value of 0.52 was determined from the fit. Inspection of the best fit lines indicate that Scheme 1 does not adequately describe the data. Upon inspection, the most striking difference between the simulation from Scheme 1 and the experimental time courses is that the experimental time courses exhibit variable peak height and not the uniform decrease exhibited in the simulation. This observation indicates that the formation and disappearance of each intermediate is not governed by the same rate constants.

The variability in the peak height suggests that each incorporation is governed by a different rate constant. To test this hypothesis, Fig. 2 Scheme 2 is a minimally modified version of Scheme 1 and contains a unique  $k_{obs}$  for each incorporation. Scheme 2 was used to simulate the time courses shown in Fig. 2 C. As expected, variability in the peak height was observed depending on the rate constant values simulated. Unlike Fig. 2 A, the maximal peak height for the intermediate time courses shown in Fig. 2 C do not follow a systematic decrease in the maximal peak height. Rather, the peak heights exhibit variability depending on the choice of rate constants used for the simulation, consistent with the experimental observations. However, formation of the 19-mer still approaches unity in the simulated time courses, whereas experimentally the time course approaches  $\sim 0.8$ .

The parameters in Scheme 2 with the additional global amplitude scalar were optimized to describe the experimental data shown in Fig. 1 C. The best fit lines and experimental data are shown in Fig. 2 D. Inspecting the time courses and corresponding fit lines reveals there is a dramatic increase in the quality of the fits as compared with Scheme 1. This is further supported by the change in the  $\chi^2$  from 0.52 using Scheme 1 to 0.06 using Scheme 2.

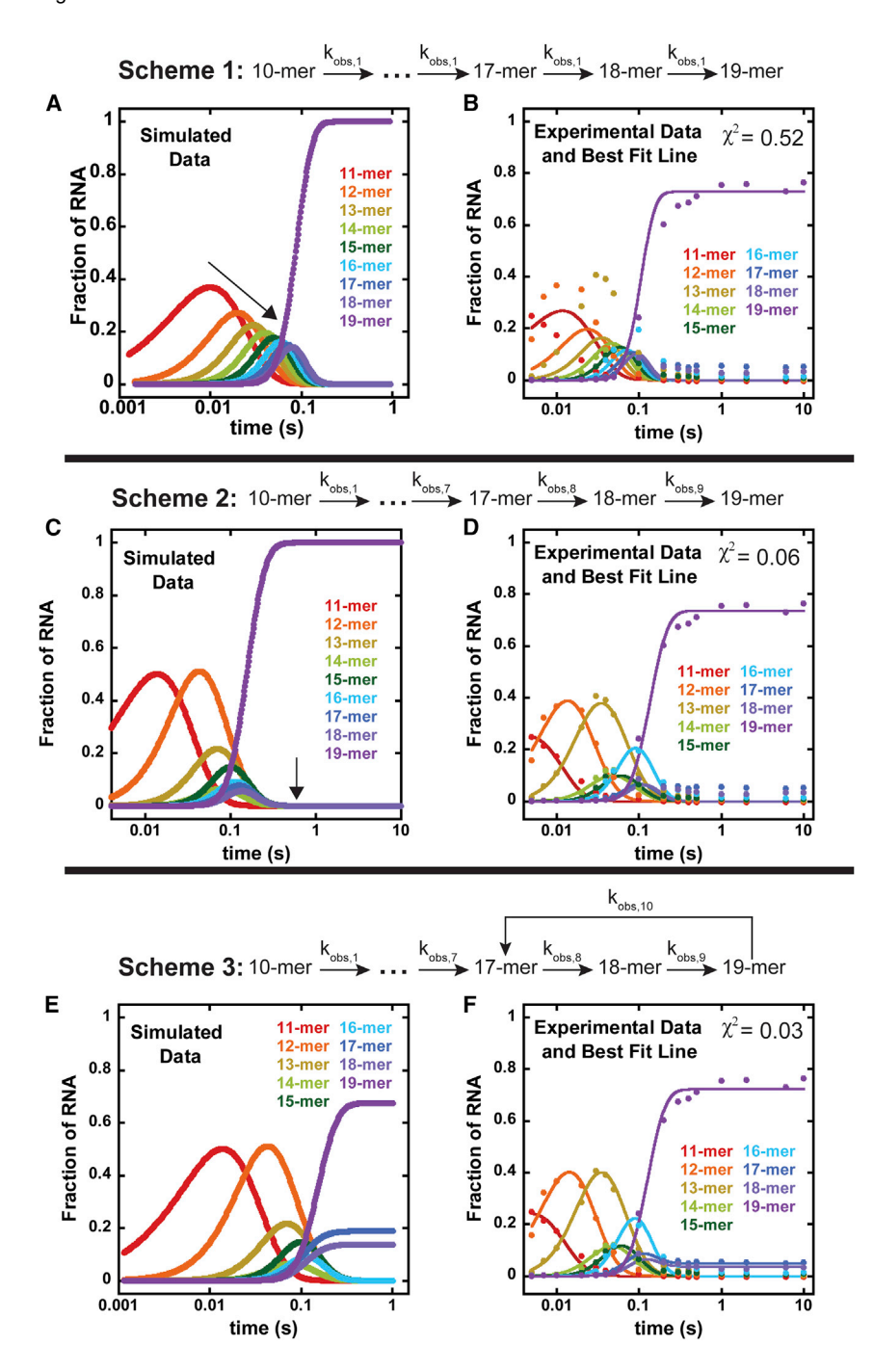


FIGURE 2 Evolution of the final scheme used to describe the experimental data. (A) Simulated time courses using Scheme 1, in which the  $k_{obs}$  for each incorporation event was identical. A systematic decrease in the maximal peak height was observed for each intermediate. (B) Experimental 1 mM ATP and 1 mM GTP time courses for each RNA intermediate and best fit lines when fit to Scheme 1 with an additional global scalar. (C) Simulated time courses using Scheme 2 in which the  $k_{obs}$  for each intermediate is different. A feature of this scheme is that no intermediates have a plateau after the rise phase and varying maximal amplitudes are observed for different intermediates. (D) Experimental 1 mM ATP and 1 mM GTP time courses and best fit lines when fit to Scheme 2 with an additional global scalar. (E) Simulated time courses from Scheme 3 in which an additional parameter  $k_{obs,10}$  is added. Time courses for 17-mer and 18-mer have a plateau after rise phase. (F) Experimental time courses from 1 mM ATP and 1 mM GTP experiment and best fit lines when fit to Scheme 3. To see this figure in color, go online.

However, the 17-mer and 18-mer time courses are not well described at time points  $>\sim 0.3$  s. The time courses appear to plateau at around  $\sim 0.1$  instead of returning to zero as predicted by the simulated time courses.

As we have previously reported, when the next cognate nucleotide is not available, Pol I will backtrack and cleave a dinucleotide product (9,10,13,15–17). In the experiment described in Fig. 1, at the 19-mer position, the next cognate nucleotide is not present in the reaction. Thus, Pol I will cleave a dinucleotide product to produce a 17-mer. Once the 17-mer product is formed it is available as a substrate to reincorporate the nucleotide encoded at position 18 and 19 and repeat the process. This cleavage activity is identical to what was observed in single-nucleotide incorporation reactions with the exception that in single-nucleotide addition experiments the cleavage of the dinucleotide product produces a substrate RNA that is no longer radio labeled (9,10,13,15,17). With the cleavage reaction in mind, Fig. 2 Scheme 3 was constructed to account for the cleavage that would occur at the end by adding  $k_{obs,10}$  to Scheme 2. In

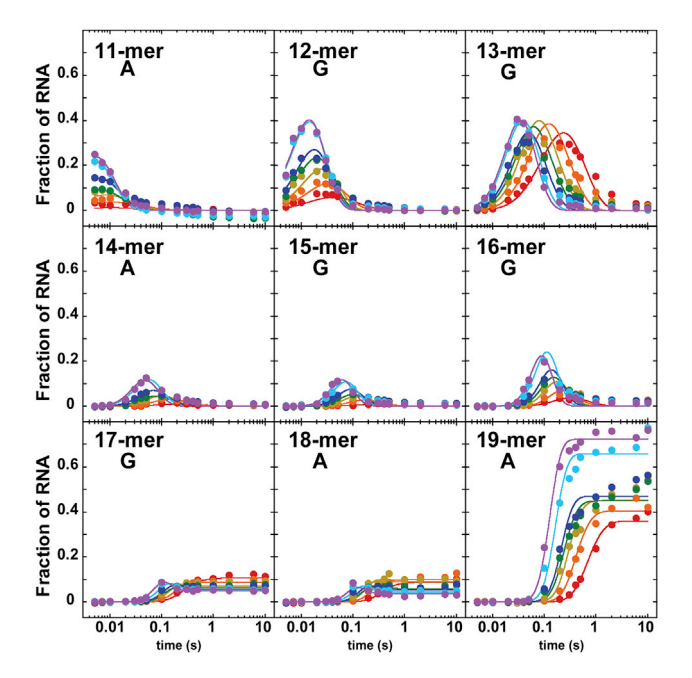


FIGURE 3 Representative set of time courses of 11-mer to 19-mer with varying [ATP], whereas [GTP] is held constant at 1 mM. The colors red, orange, gold, green, dark blue, light blue, and purple correspond to 10, 20, 50, 100, 200, 600, and 1000  $\mu$ M ATP, respectively. The identity of the RNA intermediate being monitored is written in the top left corner along with the identity of the NMP being incorporated. Time courses arising from a given [ATP] and 1 mM GTP were fit globally across all intermediates using Scheme 3 located in Fig. 2. The best fit line for each fit is shown with the corresponding time course. To see this figure in color, go online.

Scheme 3, the parameter  $k_{obs,10}$  is the rate constant for cleavage of the 19-mer to produce a 17-mer. This 17-mer reenters into the reaction path and again can be extended to form an 18-mer and 19-mer. This also accounts for the fact that the experimental time courses for the 17- and 18-mer do not completely return to baseline like other intermediates in the reaction pathway.

Inclusion of the cleavage step with rate constant  $k_{obs,10}$  in the scheme gives rise to plateaus of the 17-mer and 18-mer time courses as shown in Fig. 2 E. Although experimentally a modest plateau is observed,  $\sim 0.1$ , the parameters chosen for the simulations shown in Fig. 2 E were purposefully chosen to clearly demonstrate this plateau feature. The parameters in Scheme 3, with an additional global scalar, were globally optimized to describe the experimental time courses shown in Fig. 1 C. The time courses and corresponding best fit lines are shown in Fig. 2 F. Inclusion of the  $k_{obs,10}$ step resulted in the  $\chi^2$  dropping from 0.06 in Fig. 2 D to 0.03 shown in Fig. 2 F. Individual intermediate time courses and the corresponding best fit lines are shown in Fig. S1. This minimal model was not further modified because all observed time course features were described by the best fit lines.

The single turnover nucleotide incorporation experiments discussed here are sensitive to the slowest step in each

repeating cycle of nucleotide addition. However, the exact identity of that kinetic step remains unclear. To begin to reveal information on the identity of the rate-limiting step, we examined the ATP and GTP concentration dependence of the kinetic mechanism. Under the conditions of 1 mM GTP and 1 mM ATP, it is expected that nucleotide binding is fast; therefore, lowering the nucleotide concentration will identify if the rate-limiting step is nucleotide binding, a step coupled to nucleotide binding, or something else (13). First, the [ATP] was varied from 10  $\mu$ M to 1 mM whereas the [GTP] was held constant at 1 mM. A representative set of time courses are shown in Fig. 3. The second set of experiments were similarly carried out varying [GTP] from 10  $\mu$ M to 1 mM, whereas the concentration of ATP was held at 1 mM. A representative set of each of the time courses in which the [GTP] was varied is shown in Fig. S2. The best fit lines shown in Fig. 3 and Fig. S2 were generated from optimizations using Scheme 3. The top left corner of each panel of Fig. 3 and Fig. S2 contains the RNA intermediate being observed and the identity of the nucleotide being incorporated. Each intermediate in Fig. 3 and Fig. S2 have the expected rise and fall phase. In contrast, the final RNA product, 19-mer, exhibits a rise and plateau.

# Quantitative analysis of transcription time courses

The parameters in Scheme 3 were globally optimized to describe all time courses, 11-mer to 19-mer, for a given [ATP]/[GTP] pair, and the best fit lines are shown in Fig. 3 and Fig. S2. Time courses illustrating the appearance of the 11-mer to 19-mer for a given [ATP]/[GTP] pair were fit globally using Scheme 3. Replicate time courses were all fit to Scheme 3 independently, and the fit parameters for each [ATP]/[GTP] pair were tabulated. The mean and standard deviations were calculated from the replicate fit parameters. The resultant values are plotted as a function of [ATP] in Fig. 4 and as a function of [GTP] in Fig. 5.

Panels A–I shown in Figs. 4 and 5 correspond to the first nine  $k_{obs}$  parameters present in Scheme 3. The  $k_{obs}$  parameters describe nine different nucleotide additions, 10-mer to 19-mer. The identity of the nucleotide being incorporated at each position is displayed in the top right corner of each panel. Fig. 4, A, D, H,  $and\ I$  correspond to AMP incorporations and exhibit an [ATP] dependence, whereas Fig. 4, B, C,  $and\ E$ –G correspond to GMP incorporations and are independent of [ATP].

Inspection of the four secondary plots exhibiting an [ATP] dependence suggested a hyperbolic dependence, which is consistent with rapid equilibrium binding of the nucleotide. Equation 1 represents a proposed mechanism for each incorporation in which E is the Pol I elongation complex that binds to the incoming nucleotide substate, S. Under rapid equilibrium conditions, it is assumed that  $k_2$  is much faster than  $k_3$ . Consequently, nucleotide is assumed

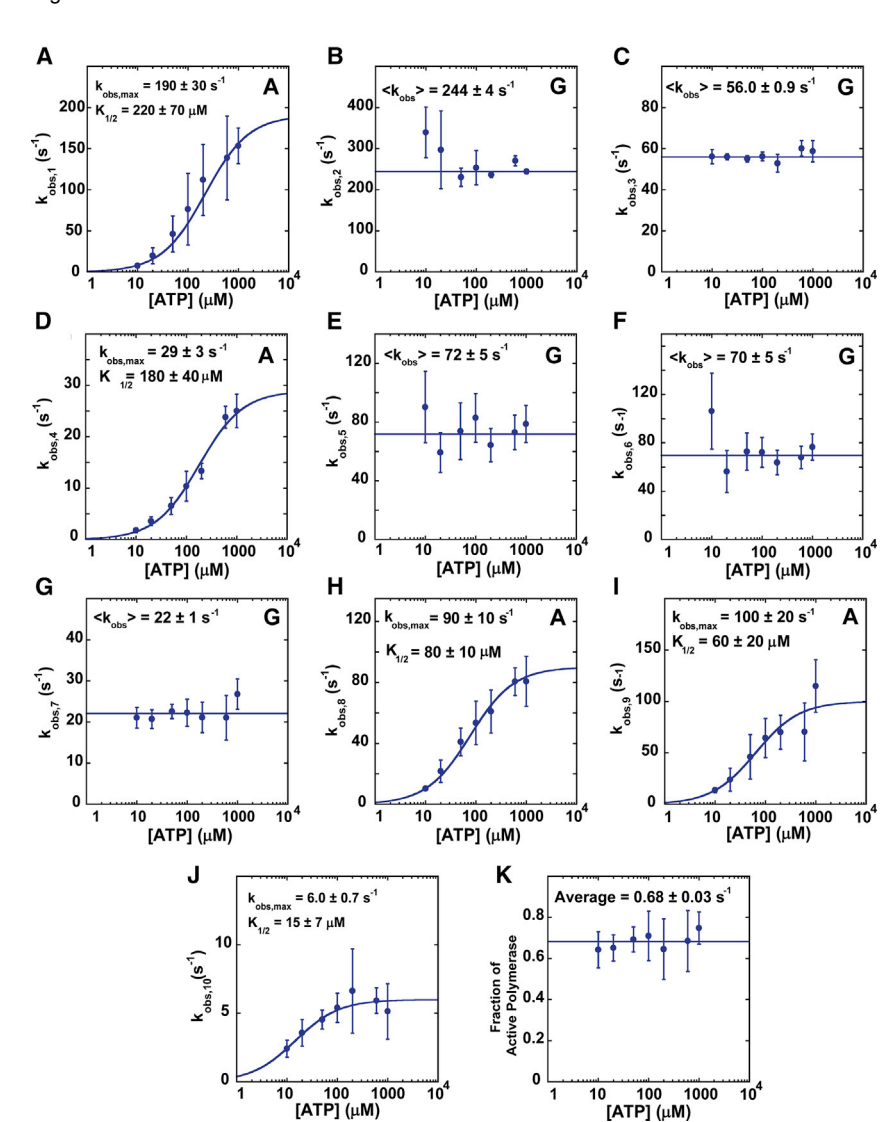


FIGURE 4 Secondary plots of Scheme 3 optimized parameters describing time courses from different [ATP] conditions. The data points are the mean values of each parameter at a specified [ATP] and the error bars are the standard deviations. Secondary plots exhibiting an [ATP] dependence were fit with a rectangular hyperbola and the best fit line is shown with the respective data set. The weighted mean value was calculated for secondary plots which did not exhibit an [ATP] dependence.  $\langle k_{obs} \rangle$  indicates the weighted average  $k_{obs}$ . (A-I) The panels correspond to the first nine  $k_{obs}$  rate constants present in Scheme 3. The identity of the nucleotide being incorporated is shown in the top right corner of each panel. (J) This secondary plot displays how [ATP] impacts the nuclease activity,  $k_{obs,10}$ , of Pol I. (K) Plot of fraction of active elongation complex with varying [ATP]. To see this figure in color,

to both bind and dissociate frequently and each addition cycle would be rate limited by  $k_3$ . The S dependence on the rate of reaction to form  $(E \bullet S)^*$  is described by Eq. 2. A derivation of this equation and accompanying discussion has been previously published (18). Here, we will point out two considerations for interpretations using this equation. First, the irreversible reaction occurs immediately after substrate binding and an undetected fast step cannot exist between the binding step and step with rate constant, k<sub>3</sub>. Second, the exact identity of this reaction step is unclear from this analysis alone:

$$E + S \underset{k_2}{\overset{k_1}{\rightleftharpoons}} E \bullet S \xrightarrow{k_3} (E \bullet S)^*$$
 (1)

$$k_{obs} = \frac{k_{obs,max}[S]}{K_{1/2} + [S]}$$
, where  $K_{1/2} \approx \frac{k_2}{k_1}$  and  $k_3 = k_{obs,max}$  (2)

The four secondary plots exhibiting an [ATP] dependence were subjected to analysis using the above rectangular hyperbola (Eq. 2), in which the parameters  $k_{obs,max}$  and  $K_{1/2}$ were optimized to describe the experimental data. The weighted average,  $\langle k_{obs} \rangle$ , was determined for each isotherm that did not exhibit a [NTP] dependence. Strikingly, although the four secondary plots are all describing AMP incorporation, we observed variability in the affinity for ATP, i.e.,  $K_{1/2}$ , as well as the maximal rate constant,  $k_{obs,max}$ . Thus, each AMP incorporation event appears to possess both a different maximal rate constant and nucleotide-binding affinity.

Fig. 4, B, C, and E-G and Fig. 5, B, C, and E-G all correspond to  $k_{obs}$  parameters describing GMP incorporation. In Fig. 5, these parameters exhibited a [GTP] dependence similar to the AMP incorporations discussed above. The secondary plots exhibiting a [GTP] dependence were likewise subjected to analysis using a rectangular hyperbola (Eq. 2).

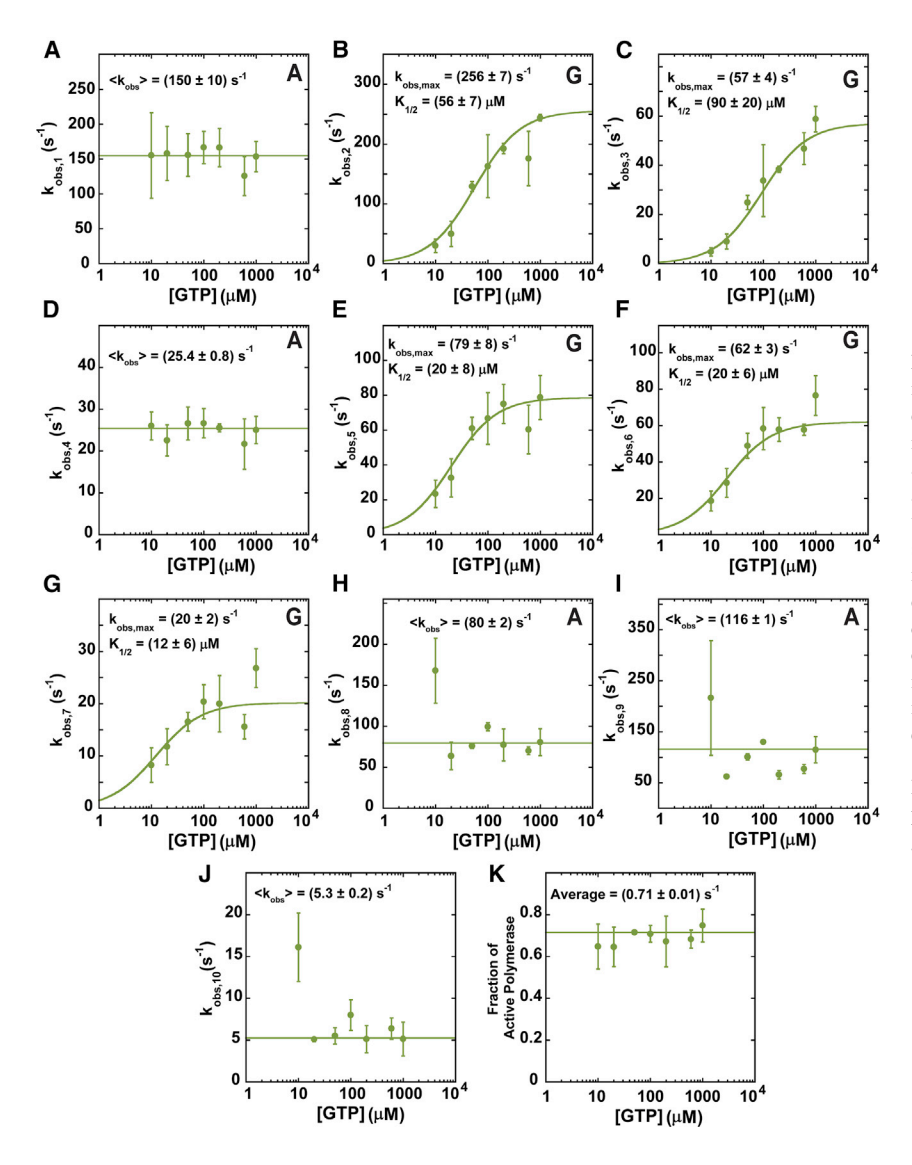


FIGURE 5 Secondary plots of Scheme 3 optimized parameters describing time courses from different [GTP] conditions. The data points are the mean values of each parameter at a specified [GTP] and the error bars are the standard deviation. Secondary plots exhibiting a [GTP] dependence were fit with a rectangular hyperbola and the best fit line is shown with the respective data set. The weighted mean value was calculated for secondary plots which did not exhibit a [GTP] dependence.  $\langle k_{obs} \rangle$  indicates the weighted average  $k_{obs}$ . (A-I) The panels correspond to the first nine  $k_{obs}$  rate constants present in Scheme 3. The identity of the nucleotide being incorporated is shown in the top right corner of each panel. (J) This secondary plot displays how [GTP] impacts the nuclease activity,  $k_{obs,10}$ , of Pol I. (K) Plot of fraction of active elongation complex with varying [GTP]. To see this figure in color, go online.

The  $k_{max}$  and  $K_{1/2}$  values exhibited variability, indicating that the rate constant of GMP incorporation and GMP affinity are different at different incorporation positions.

Figs. 4 J and 5 J display isotherms of  $k_{obs,10}$ , which, in Scheme 3, is the rate constant describing cleavage of the 19-mer to a 17-mer. Interestingly in Fig. 4 J, this isotherm exhibits an [ATP] dependence with a  $K_{1/2}$  of  $\sim$ 15  $\mu$ M and a  $k_{max}$  of  $\sim 6$  s<sup>-1</sup>. As shown in Fig. 5 J, the parameter did not exhibit a [GTP] dependence. It was originally hypothesized that this observation is a consequence of the last two nucleotide incorporations both being AMP. This hypothesis was tested by simulation; however, as shown in the Supporting materials and methods, an [ATP] dependence was not observed for  $k_{obs,10}$ . This finding suggests that ATP, but not GTP, is coupled to the nuclease activity of Pol I.

Figs. 4 K and 5 K are plots of the global scalar that was applied to each set of nine time courses resulting from a given transcription experiment. This scalar describes the fraction of active elongation complexes that elongate the RNA primer. This parameter did not exhibit an [ATP] nor [GTP] dependence and was  $\sim 0.7$  across all experiments. This parameter indicates that  $\sim$ 70% of the elongation complexes that incorporated the radiolabeled CTP in the 3' labeling step were intact and able to catalyze the addition of the subsequent nucleotides.

Greater parameter uncertainty was observed at lower [NTP] compared with higher [NTP] in several panels shown in Figs. 4 and 5. Consider the deviation present at 10  $\mu$ M ATP in Fig. 4 B. At 10  $\mu$ M ATP the preceding incorporation (Fig. 5 A) is "slow" ( $\sim$ 5 s<sup>-1</sup>) compared with the "fast" incorporation observed in Fig. 4 B ( $\sim$ 320 s<sup>-1</sup>). This "slow" step followed by a "fast" step results in no buildup of the intermediate and results in greater parameter uncertainty. Now consider Fig. 4 C at 10  $\mu$ M ATP. The  $k_{obs}$  for this step is "fast" ( $\sim 56 \text{ s}^{-1}$ ) relative to the next  $k_{obs}$  shown in Fig. 4 D ( $\sim 2$  s<sup>-1</sup>). A "fast" step followed by a "slow"

TABLE 1 Tabulated secondary plot fit parameters shown in Figs. 4 and 5

	Varying [ATP] and saturating [GTP] <sup>a</sup>			Saturating [ATP] and varying [GTP] <sup>b</sup>		
	$k_{obs,max}$ (s <sup>-1</sup> )	$K_{I/2}$ ( $\mu$ M)	$\langle k_{obs} \rangle$ (s <sup>-1</sup> )	$k_{obs,max}$ (s <sup>-1</sup> )	$K_{I/2}$ ( $\mu$ M)	$\langle k_{obs} \rangle$ (s <sup>-1</sup> )
k <sub>obs,1</sub> - A	190 ± 30	220 ± 70	_	_	_	150 ± 10
k <sub>obs,2</sub> - G	_	_	$244 \pm 4$	$256 \pm 7$	$56 \pm 7$	_
k <sub>obs,3</sub> - G	_	_	$56 \pm 0.9$	$57 \pm 4$	$90 \pm 20$	_
k <sub>obs,4</sub> - A	$29 \pm 3$	$180 \pm 40$	_	_	_	$25.4 \pm 0.8$
k <sub>obs,5</sub> - G	_	_	$72 \pm 5$	$79 \pm 8$	$20 \pm 8$	_
k <sub>obs,6</sub> - G	_	_	$70 \pm 5$	$62 \pm 3$	$20 \pm 6$	_
k <sub>obs,7</sub> - G	_	_	$22 \pm 1$	$20 \pm 2$	$12 \pm 6$	_
k <sub>obs,8</sub> - A	$90 \pm 10$	$80 \pm 10$	_	_	_	$80 \pm 2$
k <sub>obs,9</sub> - A	$100 \pm 20$	$60 \pm 20$	_	_	_	$116 \pm 1$
k <sub>obs,10</sub> - Nuclease	$6.0 \pm 0.7$	$15 \pm 7$	_	$5.3 \pm 0.2$	_	_

<sup>&</sup>lt;sup>a</sup>Isotherms in which the [ATP] was varied. Reported parameter and uncertainty values were generated by taking the mean and standard deviation of two or more experimental replicates.

step results in a buildup of the intermediate (demonstrated in the 13-mer time course shown in Fig. 3). The buildup of this intermediate is better described in fitting analysis and results in smaller parameter uncertainty values. To summarize, a "slow" step followed by a "fast" step results in an increase in parameter uncertainty. However, a "fast" step followed by a "slow" step results in a decrease in the parameter uncertainty. The time courses present in this manuscript have a mixture of these two different cases, resulting in variability in parameter uncertainty values for each incorporation.

The  $k_{max}$  and  $K_{1/2}$  values for each NMP incorporation in Figs. 4 and 5 are tabulated in Table 1. The left most column contains the  $k_{obs}$  parameters describing the nine NMP incorporations and the identity of the NMP being incorporated at each position. The next three columns correspond to the case in which the [ATP] was varied, whereas the [GTP] was held at saturating conditions of 1 mM. The last three columns correspond to the kinetic parameters in the case of saturating conditions of 1 mM ATP with varying [GTP].

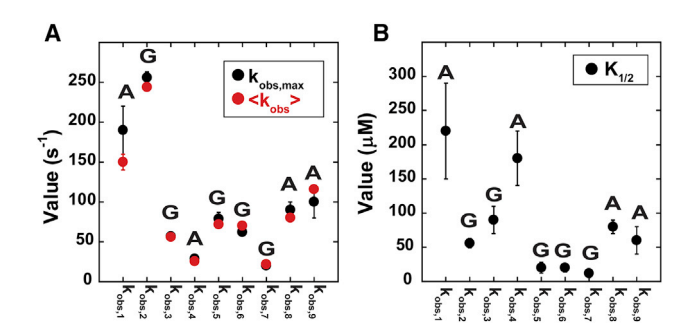


FIGURE 6 Secondary plot fit parameters shown in Figs. 4 and 5 for the first nine  $k_{obs}$  parameters. (A) Plot of  $k_{max}$  and  $\langle k_{obs} \rangle$  parameter values for each  $k_{obs}$  parameter. The identity of the nucleotide being incorporated is written above each  $k_{obs}$  parameter. Reported parameter and uncertainty values were generated by taking the mean and standard deviation of two or more experimental replicates. Parameter errors were identical to those shown in Figs. 4 and 5. (B)  $K_{1/2}$  values for the first nine  $k_{obs}$  parameters. Errors were identical to those found in Figs. 4 and 5. To see this figure in color, go online.

An overlay of the different  $k_{max}$  and  $\langle k_{obs} \rangle$  values is shown in Fig. 6 A along with the  $K_{1/2}$  values in Fig. 6 B. The excellent agreement between the  $k_{max}$  and  $\langle k_{obs} \rangle$  values indicates that the constant parameters shown in Figs. 4 and 5 correspond to the k<sub>max</sub> for the NMP being incorporated. For instance, the first incorporation is an AMP and is described by  $k_{obs,I}$ . This parameter exhibits an [ATP] dependence and has a  $k_{max}$  of  $\sim 190 \text{ s}^{-1}$ . The parameter does not exhibit a [GTP] dependence, but in the presence of saturating ATP, also exhibits a  $< k_{obs} >$  of  $\sim 150 \text{ s}^{-1}$ . Thus, the concentration of other nucleotides in solution do not significantly impact the kinetics of the NMP being incorporated. However, there is a striking level of variability in the kinetics at different nucleotide incorporation positions as demonstrated by the  $k_{max}$ ranging from  $\sim$ 20 to  $\sim$ 256 s<sup>-1</sup>, shown in Fig. 6 A and the  $K_{1/2}$  values ranging from  $\sim$ 12 to  $\sim$ 220  $\mu$ M shown in Fig. 6 B.

The specificity constant,  $k_{obs,max}/K_{1/2}$ , was calculated for each of the nine nucleotide incorporations and is shown in Fig. S5. The values ranged from (0.2 to 4.6)  $\mu M^{-1}$  s<sup>-1</sup>. No clear trend was observed based on the identity of the nucleotide being incorporated, but a possible repeating cycle was observed in which the ratio appears to rise and fall every four nucleotides. A similar repeating cycle has been observed in Escherichia coli RNAP (19).

#### DISCUSSION

Here we have shown how the [ATP] and [GTP] impact the kinetics of nucleotide addition catalyzed by Pol I. Experiments deducing full [ATP] and [GTP] dependences resulted in well-defined  $k_{obs,max}$  and  $K_{1/2}$  values at each of the nine sequential nucleotide additions. We identified that the rate-limiting step immediately follows nucleotide binding. We have additionally demonstrated that Pol I exhibits kinetic variability in both  $k_{obs,max}$  and  $K_{1/2}$  values depending on the incorporation positions. Interestingly, the  $k_{obs,max}$ values for the first two nucleotide incorporations were shown to be much faster than subsequent NTP additions.

bIsotherms in which the [GTP] was varied. Reported parameter and uncertainty values were generated by taking the mean and standard deviation of two or more experimental replicates.

Additionally, the  $K_{1/2}$  values of GMP incorporation are smaller compared with AMP suggesting tighter affinity for the GTP substrate compared with ATP.

Monitoring nine sequential nucleotide additions in this study has revealed new details regarding the mechanism of nucleotide incorporation. The rate constant for the first incorporation in these multinucleotide addition experiments is the same as the rate constant detected in previous singlenucleotide addition studies (13). Strikingly, this observation is in contrast to previous studies of E. coli RNAP in which the presence of nontemplated NTPs resulted in an increase in the templated NTP incorporation kinetics (20,21). Interestingly, the second nucleotide addition was also fast (220 s<sup>-1</sup>), which would not be known from single-nucleotide incorporation experiments alone. However, the remaining nucleotide additions decrease to a value consistent with the  $\sim 60$  nt s<sup>-1</sup> observed from averaging many incorporations (9). This observation supports the idea that the kinetics of individual incorporations determined in this experimental strategy are an accurate representation of what would be occurring during processive transcription. It is not surprising that the first two fast incorporations would not show up in averages over hundreds or thousands of additions that are close to  $\sim 60$  nt s<sup>-1</sup>. These observations reveal the importance of interrogating the mechanisms of individual incorporations during processive elongation to complement what we have learned from examining the averages over thousands of incorporations.

Illustrated in Fig. 6 A, the A at position four and the G at position seven both have reduced  $k_{max}$  values. Interestingly, the preceding two encoded nucleotides in both cases are G. This suggests that the nucleotide incorporation kinetics of Pol I may be partially governed by sequence-dependent effects. Interestingly, Pol II did not exhibit a reduction in the  $k_{obs}$  at identical incorporation positions (10).

The time courses and analysis presented here indicate that Pol I NTP binding is described as a rapid equilibrium process. Each of the secondary plots show in Figs. 4 and 5 exhibit a rectangular hyperbolic dependence on the incorporated nucleotide. This dependence indicates that the rate-limiting step is coupled to nucleotide binding. The average  $K_{1/2}$  across the nine NMP incorporations shown in Table 1 is (80  $\pm$  70)  $\mu$ M. Assuming that NTP binding is a diffusion-limited process occurring with a rate constant ≈  $(1 \times 10^8) \text{ M}^{-1} \text{ s}^{-1}$  and that the  $K_{1/2}$  values are approximately equal to NTP dissociation equilibrium constants, then NTP release values range from  $(1 \times 10^3)$  s<sup>-1</sup>to  $(2 \times 10^4)$  s<sup>-1</sup>. Each of the rate constant values in this range are well within the rapid equilibrium regime with respect to the next step in the pathway (i.e.,  $k_{NTP, binding}$  >  $k_{NTP, dissociation} >> k_{obs}$ ). This kinetic attribute is consistent with other polymerases and suggests partial mechanistic conservation across polymerases (9,13,16,22,23).

Because we have examined the kinetic mechanism at nucleotide concentrations that are both well above and below

the  $K_{1/2}$ , we are able to independently determine the maximal rate constant at saturating nucleotide, k<sub>max</sub>, and the concentration of nucleotide to achieve halfof the maximal rate constant,  $K_{1/2}$ . This contrasts with studies only performed at nucleotide concentrations below the  $K_{1/2}$  in which one only has better constraints on the ratio,  $k_{max}/K_{1/2}$ . For comparison to other studies, Fig. S5, shows the values for  $k_{obs,max}/K_{1/2}$ calculated for each of the nine nucleotide incorporations. The average value was determined to be  $(2.0 \pm 0.5) \,\mu\text{M}^{-1}\,\text{s}^{-1}$  or  $(2.0 \pm 0.5) \times 10^6 \,\mathrm{M}^{-1}\,\mathrm{s}^{-1}$ . This value is consistent with what has been observed in other DNA and RNAPs (9,24–27).

This parameter,  $k_{max}/K_{1/2}$  or  $k_{cat}/K_{m}$  is often interpreted to be the second order rate constant. Using Eq. 2 we can define  $k_{max}/K_{1/2} = k_3 \times (k_1/(k_2 + k_3))$ . What this reveals is that  $k_{max}/K_{1/2}$  is only the bimolecular rate constant in the limit of  $k_3 >> k_2$ . However, this violates the rapid equilibrium assumption, which requires  $k_2 >> k_3$ . This leads to the obvious question of whether the rapid equilibrium assumption is a good assumption for our system or is it possible that the dissociation of nucleotide is much slower than the rate constant that follows nucleotide binding. How does one test the rapid equilibrium assumption? The observation of a rectangular hyperbolic dependence on substrate concentration is evidence for rapid equilibrium binding, which is what we detect in our system. Thus, under rapid equilibrium conditions,  $k_2 >> k_3$ , it cannot be simultaneously true that  $k_3 >> k_2$ . Therefore, under our conditions  $k_{max}/K_{1/2} = k_3 \times (k_1/k_2)$ . Because this parameter is often interpreted as the bimolecular rate constant, k1, the better way to think of this ratio is as  $k_1 \times (k_3/k_2)$ . Under rapid equilibrium conditions the ratio  $k_3/k_2$  is always less than one because  $k_2 >> k_3$ . Consequently, the bimolecular rate constant,  $k_1$ , is always scaled down by the ratio  $k_3/k_2 << 1$ . These two extremes  $(k_2 >> k_3 \text{ vs. } k_3 >> k_2)$  taken together reveal that the  $k_{max}/K_{1/2}$  value represents a lower limit on the bimolecular rate constant, i.e., the true bimolecular rate constant cannot be slower than  $k_{max}/K_{1/2}$  but it could be much faster. Our results in Fig. S5 are consistent with this idea and show that this parameter is two orders of magnitude smaller than the diffusion limit value of the bimolecular rate constant  $\sim (1 \times 10^8) \text{ M}^{-1} \text{ s}^{-1}$ . Similarly, we reported a  $k_{max}$  and  $K_{1/2}$  for steady-state measurements of Pol I nucleotide incorporation averaged over hundreds of incorporations (9). The  $k_{max}/K_{1/2} = ((67 \pm 4)/(142 \pm 22)) \text{ mM}^{-1} \text{ s}^{-1} \text{ or}$  $(0.47 \pm 0.08) \times 10^6 \,\mathrm{M}^{-1} \,\mathrm{s}^{-1}$ , which is closer to the low end of what is reported here.

Interestingly, a similar study monitoring sequential nucleotide incorporations catalyzed by E. coli RNAP observed a similar rise and fall pattern of  $k_{max}/K_{1/2}$  compared with what was observed in this study (19). The authors monitored nine successive NTP additions within the initiation phase of transcription. They observed a cycle for every three nucleotides incorporated in the plot of  $k_{max}/K_{1/2}$  and concluded that the patterns are caused from stress buildup between the polymerase and the promoter sequence. This stress increases until there is a disruption in the interactions between the polymerase and promoter and additional promoter DNA becomes available to absorb the stress of the next translocation step. Several single-molecule studies aid the researchers in coming to this conclusion that have not yet been performed in Pol I (28,29). Thus, we conclude that it is certainly possible that stress is being built up by the Pol I enzyme as was reported in *E. coli* RNAP, but more work is needed to make this conclusion for Pol I.

Each round of nucleotide addition contains, at minimum, four kinetic steps: nucleotide binding, covalent bond formation, pyrophosphate release, and translocation (a specific conformational change). As shown in Fig. 2, we only detect a single rate-limiting step per incorporation. Because we know multiple steps must occur for each incorporation this observation indicates that the single observed rate constant is at least an order of magnitude slower than other kinetic steps present within each incorporation cycle. Although this analysis does not directly reveal the identity of the rate-limiting step, it narrows the pool of possibilities. The rate-limiting step cannot be NTP binding because plots of the  $k_{obs}$  vs. [NTP] resulted in the rectangular hyperbolas observed in Figs. 4 and 5, which indicates that the ratelimiting step follows ATP binding. The rate-limiting step cannot be pyrophosphate release because hydrolysis must happen first, and we know the observed step immediately follows nucleotide binding. Thus, the step is either the bond formation step or a conformational change step, in which a conformation change could also be defined as translocation.

Previous examinations of Pol I single-nucleotide addition concluded that the rate-limiting step is the formation of the phosphodiester bond, however the published results come from single-nucleotide incorporation experiments that may or may not be sensitive to the translocation step (9,13). As indicated, the first two incorporations in these multinucleotide addition experiments are faster than the subsequent additions. Consequently, for reasons that remain unclear, the rate-limiting step that defines the first two incorporations may be different from the subsequent additions.

The "thio-effect" is a measure of how the NTP analogs Sp-NTP- $\alpha$ -S impact the  $k_{obs}$  for a given polymerase. If the ratio of  $k_{obs,NTP}/k_{obs,Sp-NTP-\alpha-S}$  is  $\sim 10$  or larger, then the formation of the phosphodiester bond is likely the rate-limiting step. On the other hand, a value approximately equal to 1 is inconsistent with the rate-limiting step being bond formation (24,30–32). In the 1970's, the Eckstein group used this experimental strategy to show the bond formation is unlikely the rate-limiting step for E. coli RNAP (33). Subsequent biochemical and structural investigations have identified that folding of the E. coli RNAP trigger loop and trigger helices play critical roles in the observed rate-limiting step describing E. coli RNAP nucleotide addition (34).

It has previously been hypothesized that single-nucleotide addition measurements do not report on the translocation step in nucleotide addition (9,13). The absence of this kinetic step could explain the first  $k_{obs,max}$  being different compared with the others. Pol I single-nucleotide addition experiments using Sp-NTP- $\alpha$ -S revealed an  $\sim$ 35-fold reduction in the observed rate constant at saturating [NTP]. This observation is consistent with bond formation being rate limiting in the possible absence of the translocation step (9). It is possible that translocation is partially rate limiting for Pol I as it has already been proposed for Pol II, and the first  $k_{obs,I}$  is reporting on the rate-limiting step in the absence of translocation (35). However, this rationale does not explain the second  $k_{obs,max}$  being fast.

Studies on *Escherichia coli* RNAP suggest the presence of an allosteric NTP binding site that stimulates nucleotide incorporation (20,21). In those manuscripts, plots of  $k_{obs}$  versus [NTP] were sigmoidal indicating cooperative binding. The cooperative binding was concluded to indicate an allosteric NTP binding site on RNAP. As shown in Figs. 4 and 5, the plots of Pol I  $k_{obs}$  versus [NTP] were well described by either a rectangular hyperbola (Eq. 2) or a line. As shown in Figs. S3 and S4, no sigmoidal character was detected at low [NTP]. Thus, no evidence was found to support the presence of an allosteric NTP binding site for Pol I.

Transient state kinetics have also been used to study T7 bacteriophage RNAP. Those results indicate that an isomerization before bond formation is the rate-limiting step (25). In contrast, bond formation has been shown to possibly be the rate-limiting step for eukaryotic Pol I and at minimum partially rate limiting for eukaryotic Pol II (9,35,36). While all RNAPs are catalyzing nucleotide addition, clear mechanistic differences are present in each (10). Similar characterizations have not yet been performed in other RNAPs and are of immediate interest to understand the functional differences.

Many polymerase nucleotide addition studies have been performed using assays monitoring a few nucleotide incorporations (9,10,13,15–17,20,21,37–41). As shown in Fig. 6, the first two nucleotide incorporations exhibited considerably faster  $k_{obs,max}$  values. This suggests that Pol I may have initially been in a conformation that allowed for rapid nucleotide addition and this state does not reflect the kinetics of processive elongation. Taken together these observations highlight the possible concerns with research studies in which only a few nucleotide incorporations are monitored while simultaneously providing a framework for future characterizations of different RNAPs. A recent E. coli RNAP transcription publication monitoring initiation kinetics reported a similar observation in which the first nucleotide incorporated differently compared with the subsequent incorporations (19).

# **CONCLUSION**

Nine sequential rounds of nucleotide addition were monitored using reconstituted Pol I elongation complexes. Analysis of

the resultant time courses identified variability in the affinity for the incoming nucleotide and incorporation max rate constants for each incorporation. Possible repeating cycles of the ratio  $k_{obs,max}/K_{1/2}$  were identified. The identity of the rate-limiting step for Pol I nucleotide addition was also identified to be either bond formation or a conformational change. The experimental and analytical strategies implemented here provide a greater understanding of Pol I nucleotide addition and provide a framework for future investigations elucidating the mechanistic differences between all DNA-dependent RNAPs present across the three domains of life. Additional follow-up studies in which the template sequence is varied are currently underway to identify what features in the growing RNA strand or DNA template give rise to the observed rate constants.

#### SUPPORTING MATERIAL

Supporting material can be found online at https://doi.org/10.1016/j.bpj. 2021.09.008.

#### **AUTHOR CONTRIBUTIONS**

Z.M.I. wrote the manuscript and designed, performed, and analyzed experiments. A.L.L. wrote the manuscript and designed experiments. D.A.S. wrote the manuscript and designed the experiments. All authors read and approved of the final manuscript. The authors declare no competing interests.

# **ACKNOWLEDGMENTS**

We thank current and past members of the Lucius and Schneider labs for their critical discussions of the manuscript.

This work was supported by the National Science Foundation (grant NSF MCB-1817749 to A.L.L.) and National Institutes of Health (grant NIH R01 GM084946 and NIH R35 GM140710 to D.A.S.). Computational work done in data analysis was performed using the UAB High Performance Computing (HPC) Cheaha, which is supported in part by the National Science Foundation under Grants No. OAC-1541310, the University of Alabama at Birmingham, and the Alabama Innovation Fund.

# **REFERENCES**

- 1. Allison, L. A., M. Moyle, ..., C. J. Ingles. 1985. Extensive homology among the largest subunits of eukaryotic and prokaryotic RNA polymerases. Cell. 42:599-610.
- 2. Viktorovskaya, O. V., K. L. Engel, ..., D. A. Schneider. 2013. Divergent contributions of conserved active site residues to transcription by eukaryotic RNA polymerases I and II. Cell Rep. 4:974–984.
- 3. Viktorovskaya, O. V., and D. A. Schneider. 2015. Functional divergence of eukaryotic RNA polymerases: unique properties of RNA polymerase I suit its cellular role. Gene. 556:19-26.
- 4. Steinberg, T. H., D. E. Mathews, ..., R. R. Burgess. 1990. Tagetitoxin: a new inhibitor of eukaryotic transcription by RNA polymerase III. J. Biol. Chem. 265:499-505.
- 5. Malagon, F., M. L. Kireeva, ..., J. N. Strathern. 2006. Mutations in the Saccharomyces cerevisiae RPB1 gene conferring hypersensitivity to 6-azauracil. Genetics. 172:2201-2209.

- 6. Bar-Nahum, G., V. Epshtein, ..., E. Nudler. 2005. A ratchet mechanism of transcription elongation and its control. Cell. 120:183-193.
- 7. Tan, L., S. Wiesler, ..., R. O. Weinzierl. 2008. Bridge helix and trigger loop perturbations generate superactive RNA polymerases. J. Biol. 7:40.
- 8. Zhang, J., M. Palangat, and R. Landick. 2010. Role of the RNA polymerase trigger loop in catalysis and pausing. Nat. Struct. Mol. Biol. 17:99-104.
- 9. Scull, C. E., Z. M. Ingram, ..., D. A. Schneider. 2019. A novel assay for RNA polymerase I transcription elongation sheds light on the evolutionary divergence of eukaryotic RNA polymerases. Biochemistry. 58:2116-2124.
- 10. Jacobs, R. Q., Z. M. Ingram, ..., D. A. Schneider. 2021. Defining the divergent enzymatic properties of RNA polymerases I and II. J. Biol. Chem. 296:100051.
- 11. Ucuncuoglu, S., K. L. Engel, ..., L. Finzi. 2016. Direct characterization of transcription elongation by RNA polymerase I. PLoS One. 11:e0159527.
- 12. French, S. L., Y. N. Osheim, ..., A. L. Beyer. 2003. In exponentially growing Saccharomyces cerevisiae cells, rRNA synthesis is determined by the summed RNA polymerase I loading rate rather than by the number of active genes. Mol. Cell. Biol. 23:1558-1568.
- 13. Appling, F. D., A. L. Lucius, and D. A. Schneider. 2015. Transient-state kinetic analysis of the RNA polymerase I nucleotide incorporation mechanism. Biophys. J. 109:2382-2393.
- 14. Appling, F. D., and D. A. Schneider. 2015. Purification of active RNA polymerase I from yeast. In Bacterial Transcriptional Control: Methods and Protocols I. Artsimovitch and T. J. Santangelo, eds.. Springer, pp.
- 15. Appling, F. D., A. L. Lucius, and D. A. Schneider. 2017. Quantifying the influence of 5'-RNA modifications on RNA polymerase I activity. Biophys. Chem. 230:84-88.
- 16. Appling, F. D., D. A. Schneider, and A. L. Lucius. 2017. Multisubunit RNA polymerase cleavage factors modulate the kinetics and energetics of nucleotide incorporation: an RNA polymerase I case study. Biochemistry. 56:5654-5662.
- 17. Scull, C. E., A. M. Clarke, ..., D. A. Schneider. 2020. Downstream sequence-dependent RNA cleavage and pausing by RNA polymerase I. J. Biol. Chem. 295:1288-1299.
- 18. Johnson, K. A. 1992. 1. Transient-state kinetic analysis of enzyme reaction pathways. In The Enzymes D. S. Sigman, ed.. Academic Press, pp. 1–61.
- 19. Henderson, K. L., C. E. Evensen, ..., M. T. Record, Jr. 2019. RNA polymerase: step-by-step kinetics and mechanism of transcription initiation. Biochemistry. 58:2339-2352.
- 20. Holmes, S. F., and D. A. Erie. 2003. Downstream DNA sequence effects on transcription elongation. Allosteric binding of nucleoside triphosphates facilitates translocation via a ratchet motion. J. Biol. Chem. 278:35597-35608.
- 21. Foster, J. E., S. F. Holmes, and D. A. Erie. 2001. Allosteric binding of nucleoside triphosphates to RNA polymerase regulates transcription elongation. Cell. 106:243-252.
- 22. Kireeva, M. L., C. Domecq, ..., M. Kashlev. 2011. Interaction of RNA polymerase II fork loop 2 with downstream non-template DNA regulates transcription elongation. J. Biol. Chem. 286:30898-30910.
- 23. Seibold, S. A., B. N. Singh, ..., Z. F. Burton. 2010. Conformational coupling, bridge helix dynamics and active site dehydration in catalysis by RNA polymerase. Biochim. Biophys. Acta. 1799:575-587.
- 24. Patel, S. S., I. Wong, and K. A. Johnson. 1991. Pre-steady-state kinetic analysis of processive DNA replication including complete characterization of an exonuclease-deficient mutant. Biochemistry. 30:511–525.
- 25. Anand, V. S., and S. S. Patel. 2006. Transient state kinetics of transcription elongation by T7 RNA polymerase. J. Biol. Chem. 281:35677-
- 26. Benkovic, S. J., and C. E. Cameron. 1995. Kinetic analysis of nucleotide incorporation and misincorporation by Klenow fragment of Escherichia coli DNA polymerase I. Methods Enzymol. 262:257-269.

- 27. Washington, M. T., L. Prakash, and S. Prakash. 2001. Yeast DNA polymerase eta utilizes an induced-fit mechanism of nucleotide incorporation. Cell. 107:917–927.
- 28. Henderson, K. L., L. C. Felth, ..., M. T. Record, Jr. 2017. Mechanism of transcription initiation and promoter escape by E. coli RNA polymerase. Proc. Natl. Acad. Sci. USA. 114:E3032-E3040.
- 29. Yu, L., J. T. Winkelman, ..., R. H. Ebright. 2017. The mechanism of variability in transcription start site selection. eLife. 6:e32038.
- 30. Erie, D. A., O. Hajiseyedjavadi, ..., P. H. von Hippel. 1993. Multiple RNA polymerase conformations and GreA: control of the fidelity of transcription. Science. 262:867–873.
- 31. Benkovic, S. J., and K. J. Schray. 1973. 6. Chemical basis of biological phosphoryl transfer. In The Enzymes P. D. Boyer, ed.. Academic Press,
- 32. Mizrahi, V., R. N. Henrie, ..., S. J. Benkovic. 1985. Rate-limiting steps in the DNA polymerase I reaction pathway. Biochemistry. 24:4010-
- 33. Armstrong, V. W., D. Yee, and F. Eckstein. 1979. Mechanistic studies on deoxyribonucleic acid dependent ribonucleic acid polymerase from Escherichia coli using phosphorothioate analogues. 2. The elongation reaction. Biochemistry. 18:4120-4123.
- 34. Belogurov, G. A., and I. Artsimovitch. 2019. The mechanisms of substrate selection, catalysis, and translocation by the elongating RNA polymerase. J. Mol. Biol. 431:3975–4006.

- 35. Dangkulwanich, M., T. Ishibashi, ..., C. J. Bustamante. 2013. Complete dissection of transcription elongation reveals slow translocation of RNA polymerase II in a linear ratchet mechanism. eLife. 2:e00971.
- 36. Larson, M. H., J. Zhou, ..., S. M. Block. 2012. Trigger loop dynamics mediate the balance between the transcriptional fidelity and speed of RNA polymerase II. Proc. Natl. Acad. Sci. USA. 109:6555-6560.
- 37. Appling, F. D., C. E. Scull, ..., D. A. Schneider. 2018. The A12.2 subunit is an intrinsic destabilizer of the RNA polymerase I elongation complex. Biophys. J. 114:2507-2515.
- 38. Scull, C. E., A. L. Lucius, and D. A. Schneider. 2021. The N-terminal domain of the A12.2 subunit stimulates RNA polymerase I transcription elongation. Biophys. J. 120:1883-1893.
- 39. Nedialkov, Y. A., X. Q. Gong, ..., Z. F. Burton. 2003. NTP-driven translocation by human RNA polymerase II. J. Biol. Chem. 278:18303-18312.
- 40. Gong, X. Q., Y. A. Nedialkov, and Z. F. Burton. 2004. Alpha-amanitin blocks translocation by human RNA polymerase II. J. Biol. Chem. 279:27422-27427.
- 41. Zhang, C., and Z. F. Burton. 2004. Transcription factors IIF and IIS and nucleoside triphosphate substrates as dynamic probes of the human RNA polymerase II mechanism. J. Mol. Biol. 342:1085–1099.